Constant Envelope OFDM

Steve C. Thompson, *Member, IEEE,* Ahsen U. Ahmed *Student Member, IEEE,*
John G. Proakis, *Life Fellow, IEEE,* James R. Zeidler, *Fellow, IEEE,* and Michael J. Geile, *Member, IEEE*

Abstract—This paper describes a transformation technique aimed at solving the peak-to-average power ratio (PAPR) problem associated with OFDM (orthogonal frequency-division multiplexing). Constant envelope OFDM (CE-OFDM) transforms the OFDM signal, by way of phase modulation, to a signal designed for efficient power amplification. At the receiver, the inverse transformation—phase demodulation—is applied prior to the conventional OFDM demodulator.

The performance of CE-OFDM is analyzed in additive white Gaussian noise (AWGN) and fading channels. CE-OFDM is shown to achieve good performance in dense multipath with the use of cyclic prefix transmission in conjunction with a frequency-domain equalizer (FDE). By way of computer simulation and hardware realization, CE-OFDM is shown to compare favorably to conventional OFDM.

Index Terms—Constant envelope signals, OFDM, power amplifier efficiency, performance analysis.

I. INTRODUCTION

ORTHOGONAL frequency-division multiplexing is a popular modulation technique for wireless digital communications [1]–[4]. It provides a relatively straightforward way to accommodate high data rate links over harsh wireless channels characterized by severe multipath fading [5]–[8]. OFDM's primary drawback, however, is that the modulated waveform has high amplitude fluctuations that produce large peak-to-average power ratios (PAPRs) [9]–[11]. The high PAPR makes OFDM sensitive to nonlinear distortion caused by the transmitter's power amplifier (PA) [12]. Without sufficient *power backoff*, the system suffers from spectral broadening, intermodulation distortion, and, consequently, performance degradation [13]–[16]. These problems can be reduced by increasing the backoff, but this results in reduced PA efficiency [17]. For mobile battery-powered devices this is particularly an issue due to limited power resources [18]–[20]. Efficient amplification is also a critical component to future

S. C. Thompson was with the Department of Electrical and Computer Engineering, University of California, San Diego, La Jolla, CA 92093-0407 USA. He is now with Acorn Technologies, La Jolla, CA 92037 USA (e-mail: steve@elsteve.com).

A. U. Ahmed is with SPAWAR Systems Center, San Diego, CA 92152-5435 USA (e-mail: ahsen.ahmed@navy.mil). He is also with the Department of Electrical and Computer Engineering, University of California, San Diego, La Jolla, CA 92093-0407 USA.

J. G. Proakis and J. R. Zeidler are with the Department of Electrical and Computer Engineering, University of California, San Diego, CA 92093-0407 USA (e-mail: {zeidler, proakis}@ece.ucsd.edu).

M. J. Geile is with Nova Engineering, Cincinnati, OH 45246-1201 USA (e-mail: mike.geile@l-3com.com).

Digital Object Identifier 10.1109/TCOMM.2008.070043.

systems operating in the unlicensed 60 GHz band [21]. The PAPR problem is thus of great interest to both the academic and industrial communities [22], [23]. Reducing its effects is of importance to both military and commercial applications [5], [6], [8].

Many techniques have been developed to address the PAPR problem: distortionless PAPR reduction schemes such as coding and tone reservation [24]–[26]; non-distortionless PAPR reduction schemes such as clipping/filtering and peak windowing [27], [28]; predistortion schemes [29]; and receiver correction algorithms such as iterative decoding [30]. These distinctly different techniques provide different degrees of effectiveness, and present different sets of tradeoffs that may include increased complexity, reduced spectral efficiency, and performance degradation. An alternative approach to mitigating the PAPR problem is based on signal transformation. This technique involves a signal transformation prior to amplification, then an inverse transformation at the receiver prior to demodulation. In [31]–[33] a companding transform is suggested. In [21], [34]–[40] a phase modulator transform is considered. The advantage of the phase modulator transform is that the transformed signal has the lowest achievable PAPR, 0 dB. Such a signal can be amplified with minimal power backoff, which: 1) maximizes power amplifier efficiency, and 2) potentially increases system range since more signal power is radiated into the channel.

The constant envelope OFDM approach described in this paper is based on the phase modulator transform technique. In essence, the OFDM waveform is used to phase modulate the carrier. The idea of transmitting OFDM by way of angle modulation is not entirely new. In fact, Harmuth's 1960 paper suggested transmitting an OFDM-like signal by way of "amplitude or frequency modulation, or any other type of modulation suitable for the transmission of continuously varying [waveforms]" [41]. In [42] the authors suggest using existing frequency modulation (FM) infrastructure for OFDM transmission. These papers do not consider the PAPR implications, however.

The goal of the current paper is to extend the basic concept of transmitting OFDM by way of phase modulation. The CE-OFDM system described shares many of the same functional blocks as conventional OFDM. Therefore an existing OFDM system can provide an additional CE-OFDM mode with relative ease, particularly for the case of software defined platforms [43]. This point is further illustrated in Section II where the system model is explained and the relevant equations are defined.

In Section III performance analysis of CE-OFDM corrupted by additive white Gaussian noise (AWGN) is conducted. Anal-
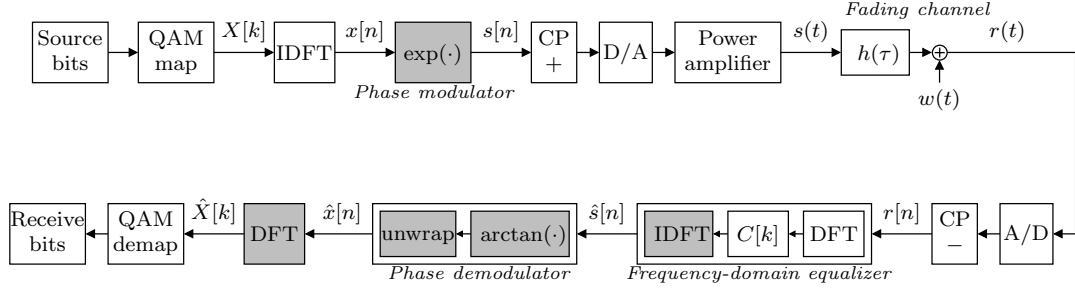
Fig. 1. Baseband CE-OFDM system model. Unshaded blocks represent those common to both conventional and constant envelope OFDM.

ysis is complicated due to the nonlinear phase demodulator preceding the OFDM demodulator. Making use of a high carrier-to-noise ratio (CNR) approximation, an expression is derived for the bit error rate (BER) that is shown to be in agreement with simulation results. The phase demodulator receiver is susceptible to the classic FM threshold effect [44], [45], which is also studied in Section III. These results lead to a spectral efficiency versus performance tradeoff study.

Section IV then extends CE-OFDM performance analysis to fading channels. For the frequency-nonselective case (Section IV-A), performance bounds are derived. For the frequency-selective case (Section IV-B) an equalization technique based on cyclic prefix transmission in conjunction with a frequency-domain equalizer (FDE) is proposed and studied over various multipath channel models. It is demonstrated that CE-OFDM, due to frequency-domain spreading of the data symbols, exploits the available multipath diversity of the channel. In Section V a comparison between conventional and constant envelope OFDM is conducted. It is shown, by way of computer simulation and hardware realization, that CE-OFDM compares favorably to conventional OFDM in the presence of PA nonlinearities. Concluding remarks are made in Section VI.

II. SYSTEM DESCRIPTION

The system under consideration is represented by the diagram in Fig. 1. During each T-second block interval, an N_{DFT}-point inverse discrete Fourier transform (IDFT) calculates a block of time samples $\{x[n]\}$. The sampling rate is therefore $F_0 = N_{\text{DFT}}/T$. To obtain a real-valued, oversampled OFDM sequence $\{x[n]\}$, the input to the IDFT is a conjugate symmetric, zero-padded data vector [46, p. 719]

$$[0, X[1], X[2], \dots, X[N_{\text{QAM}}],$$
$$\mathbf{0}_{1 \times N_{\text{zp}}}, 0, X^*[N_{\text{QAM}}], \dots, X^*[2], X^*[1]],$$

where $\{X[k]\}_{k=1}^{N_{\text{QAM}}}$ are M_{QAM}-QAM data symbols, and $\mathbf{0}_{1 \times N_{\text{zp}}}$ is an N_{zp}-element row vector comprised of zeros. The IDFT size is thus $N_{\text{DFT}} = 2N_{\text{QAM}} + N_{\text{zp}} + 2$. The zeros at index $k = 0$ and $k = N_{\text{QAM}} + N_{\text{zp}} + 1$ are used to maintain conjugate symmetry, and the remaining N_{zp} zeros achieve the effect of oversampling the time-domain sequence. The oversampling factor is defined as $C_{\text{os}} \equiv N_{\text{DFT}}/(N_{\text{DFT}} - N_{\text{zp}})$. Using this convention, the output of the IDFT may be expressed as [11,

pp. 124–126]

$$
\begin{aligned}
x[n] &= \sum_{k=0}^{N_{\text{DFT}}-1} X[k] e^{j 2\pi k n / N_{\text{DFT}}} \\
&= 2 \sum_{k=1}^{N_{\text{QAM}}} \Re\{X[k]\} \cos\left(\frac{2\pi k n}{N_{\text{DFT}}}\right) \\
&\quad - \Im\{X[k]\} \sin\left(\frac{2\pi k n}{N_{\text{DFT}}}\right),
\end{aligned}
\tag{1}
$$

$n = 0, 1, \dots, N_{\text{DFT}} - 1$, where $j = \sqrt{-1}$.

Next, $\{x[n]\}$, a high PAPR OFDM sequence [9], is passed through a phase modulator to obtain the 0 dB PAPR sequence $\{s[n] = \exp(jCx[n])\}$, where C is a scaling constant. An N_{cp}-sample cyclic prefix (CP) is appended to $\{s[n]\}$ to obtain $\{s[n]\}_{n=-N_{\text{cp}}}^{N_{\text{DFT}}-1}$, where $s[n] = s[N_{\text{DFT}} + n]$, $n = -N_{\text{cp}}, \dots, -2, -1$. The discrete-time samples are then passed through a digital-to-analog (D/A) converter, and the result is amplified and transmitted into the channel. The lowpass equivalent representation of the amplified CE-OFDM signal is $s(t) = A \exp\{j[2\pi h m(t) + \theta]\}$, $-T_{\text{cp}} \le t < T$, where A is the signal amplitude. θ is an arbitrary phase offset which may be used as a design parameter to achieve phase-continuous modulation [37]. The cyclic prefix duration is $T_{\text{cp}} = N_{\text{cp}}/F_0$ and the block duration is $T = N_{\text{DFT}}/F_0$. The information-bearing message signal $m(t)$ is a real-valued OFDM waveform having the same form as (1):

$$
\begin{aligned}
m(t) = C \sum_{k=1}^{N_{\text{QAM}}} &\Re\{X[k]\} \cos\left(\frac{2\pi k t}{T}\right) \\
&- \Im\{X[k]\} \sin\left(\frac{2\pi k t}{T}\right),
\end{aligned}
$$

$-T_{\text{cp}} \le t < T$, where C is a constant. Therefore, the phase modulating OFDM signal is comprised of $N = 2N_{\text{QAM}}$ subcarriers, each modulated by $M = \sqrt{M_{\text{QAM}}}$-ary pulse-amplitude modulation (PAM) data symbols.

It is convenient to define the message signal as $m(t) = C_{\text{norm}} \sum_{k=1}^{N} I[k] q_k(t)$, where

$$
I[k] =
\begin{cases}
\Re\{X[k]\}, & k = 1, 2, \dots, N_{\text{QAM}}, \\
-\Im\{X[k - N_{\text{QAM}}]\}, & k = N_{\text{QAM}} + 1, \dots, N,
\end{cases}
$$

$I[k] \in \{\pm 1, \pm 3, \dots, \pm(M - 1)\}$, are M-PAM data symbols,

and

$$q_k(t) = \begin{cases} \cos\left(\dfrac{2\pi k t}{T}\right), & k = 1, 2, \ldots, N_{\text{QAM}}, \\ \sin\left(\dfrac{2\pi[k - N_{\text{QAM}}]t}{T}\right), & k = N_{\text{QAM}} + 1, \ldots, N \end{cases}$$

(2)

are the subcarriers. C_{norm} is a constant used to normalize the variance of the message signal $(\sigma_m^2 = 1)$, thus making the variance of the phase signal, $\phi(t) = 2\pi h m(t)$, $\sigma_\phi^2 = (2\pi h)^2$ where h is the *modulation index*. This is achieved by setting [11, pp. 47] $C_{\text{norm}} = \sqrt{2/(N\sigma_I^2)}$, where $\sigma_I^2 = (M^2 - 1)/3$ is the variance of the independent and identically distributed data symbols [47, p. 194]. The subcarriers are centered at the frequencies $\pm i/T$ Hz, $i = 1, 2, \ldots, N/2$, so an effective double-sided bandwidth of the message signal is defined as $W \equiv N/T$ Hz. The bandwidth of $s(t)$ is lower bounded by W Hz, and a function of the modulation index. A useful bandwidth expression for the CE-OFDM signal is the RMS bandwidth [48, p. 343], [11, p. 52]

$$B = \max(2\pi h, 1)W \text{ Hz.}$$

(3)

The bit rate is $R = N \log_2 M/T$ b/s, and the spectral efficiency is

$$S = \frac{R}{B} = \frac{\log_2 M}{\max(2\pi h, 1)} \text{ b/s/Hz.}$$

(4)

The baseband representation of the received signal is $r(t) = \int_0^{\tau_{\max}} h(\tau, t)s(t - \tau)d\tau + w(t)$, where $h(\tau, t)$ is the channel impulse response with maximum propagation delay $\tau_{\max}$, and $w(t)$ is complex-valued Gaussian noise with a power density spectrum $\Phi_{ww}(f) = N_0$ over the effective bandwidth of $s(t)$ [46, p. 158]. For this study, the channel is assumed to be static relative to the transmission interval $-T_{\text{cp}} \leq t < T$. Therefore $h(\tau, t) \approx h(\tau)$, $-T_{\text{cp}} \leq t < T$. The channel impulse response is modeled as a wide-sense stationary uncorrelated scattering (WSSUS) process [49, chap. 7] comprised of L discrete paths: $h(\tau) = \sum_{l=0}^{L-1} h[l]\delta(\tau - \tau[l])$, where $h[l]$ is the complex-valued gain of the lth path. The discrete propagation delays are defined as [49, p. 269–271] $\tau[l] \equiv l/F_0$, $l = 0, 1, \ldots, L - 1$.

The received signal is first passed through an analog-to-digital (A/D) converter to obtain the samples $r[n] \equiv r(n/F_0) = \sum_{l=0}^{L-1} h[l]s[n-l] + w[n]$, $n = -N_{\text{cp}}, \ldots, N_{\text{DFT}}-1$, where $w[n] \equiv w(n/F_0)$. The cyclic prefix duration is designed such that $N_{\text{cp}} \geq L$. Consequently, $r[n]$ is expressed as

$$r[n] = \begin{cases} s[n] * h[n] + w[n], & n = -N_{\text{cp}}, \ldots, N_{\text{DFT}} - 1, \\ s[n] \circledast h[n] + w[n], & n = 0, \ldots, N_{\text{DFT}} - 1, \\ \text{DFT}^{-1}\{S[k]H[k]\} + w[n], & n = 0, \ldots, N_{\text{DFT}} - 1. \end{cases}$$

(5)

The first line in (5) represents the linear convolution between the transmitted signal samples and the channel. The second denotes circular convolution. Thus the linear and circular convolutions are equivalent for the receive samples at time indexes $n = 0, \ldots, N_{\text{DFT}} - 1$, a consequence of $N_{\text{cp}} \geq L$ in conjunction with the cyclic prefix transmission. The third line is circular convolution represented in the frequency domain [50, sec. 5.2.2]. $\text{DFT}^{-1}\{\cdot\}$ represents the IDFT operator;

$\{S[k]\}_{k=0}^{N_{\text{DFT}}-1}$ and $\{H[k]\}_{k=0}^{N_{\text{DFT}}-1}$ are the N_{DFT}-point discrete Fourier transform (DFT) of $\{s[n]\}_{n=0}^{N_{\text{DFT}}-1}$ and $\{h[n]\}_{n=0}^{L-1}$ respectively.

After the A/D converter, the cyclic prefix samples are discarded and the samples that remain, $\{r[n]\}_{n=0}^{N_{\text{DFT}}-1}$, are processed. A frequency-domain equalizer (FDE) [details of which are discussed in Section IV-B] is used to correct the distortion caused by the channel, then the operations inverse to those performed at the transmitter are performed: a phase demodulator, followed by an N_{DFT}-point DFT, followed by a symbol demapper that yields the received bits. The phase demodulator is implemented with an arctangent calculator, followed by a phase unwrapper.

As Fig. 1 indicates, the constant envelope OFDM system shares many of the same functional blocks as the conventional OFDM system. Thus an existing OFDM system can provide an additional CE-OFDM mode with relative ease.

III. Performance over AWGN Channels

For the simple AWGN case, the received signal is $r(t) = s(t)e^{j\phi_0} + w(t)$, where ϕ_0 is a phase offset caused by the channel [46, p. 301]. As indicated by the block diagram in Fig. 1, and from the development in the previous section, the CE-OFDM demodulator operates in the discrete-time domain. It is convenient, however, to consider the continuous-time model for analysis.

The output of the phase demodulator is $\hat{\phi}(t) = \phi(t) + \theta + \phi_0 + \xi(t)$, where $\xi(t) = \arctan\left[\frac{A_w(t)\sin[\phi_w(t) - \phi(t) - \theta - \phi_0]}{A + A_w(t)\sin[\phi_w(t) - \phi(t) - \theta - \phi_0]}\right]$ is a nonlinear noise component [51, p. 416]; $A_w(t) \equiv |w(t)|$ and $\phi_w(t) \equiv \arctan[w(t)]$ is the envelope and phase, respectively, of $w(t)$.

The DFT following the phase demodulator acts as a correlator bank. The kth correlator computes

$$Q[k] \equiv \frac{1}{T}\int_0^T \hat{\phi}(t)q_k(t)dt \equiv S[k] + \Psi[k] + N[k],$$

(6)

$k = 1, 2, \ldots, N$. The signal component is

$$\begin{aligned} S[k] &\equiv \frac{1}{T}\int_0^T \phi(t)q_k(t)dt \\ &= \frac{2\pi h C_{\text{norm}}}{T}\int_0^T \sum_{k'=1}^N I[k']q_{k'}(t)q_k(t)dt. \end{aligned}$$

(7)

Due to the orthogonality of the subcarriers, only the $k' = k$ term in (7) contributes, and therefore the signal component simplifies to

$$S[k] = \frac{2\pi h C_{\text{norm}}}{T}I[k]\mathcal{E}_q = 2\pi h\sqrt{\frac{1}{2N\sigma_I^2}}I[k],$$

(8)

where $\mathcal{E}_q = T/2$ is the subcarrier energy.

The term accounting for the phase offsets is

$$\Psi[k] \equiv \frac{1}{T}\int_0^T (\theta + \phi_0)q_k(t) = 0.$$

(9)

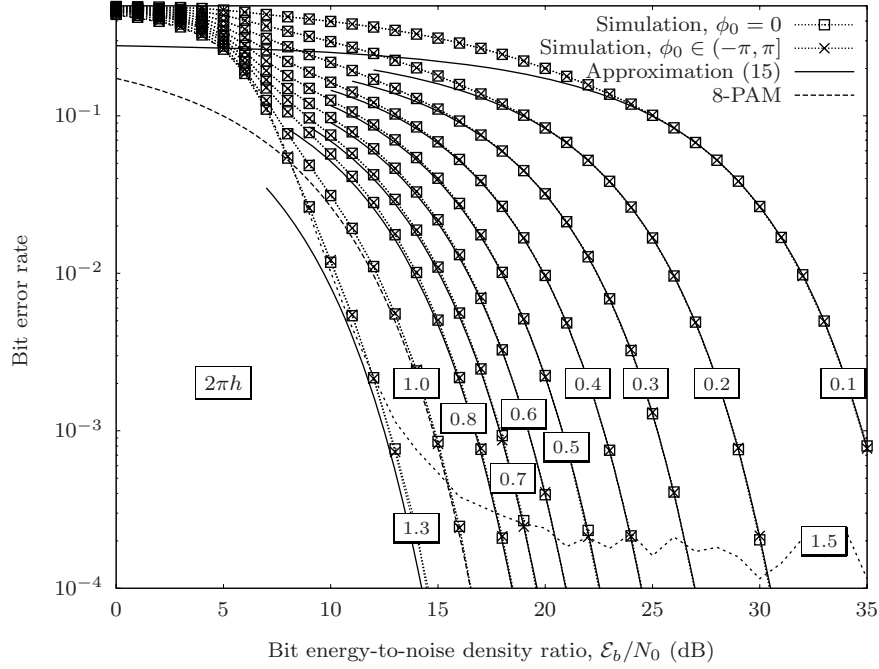Thus, due to the periodicity of the full-cycle sinusoid and cosinusoid subcarriers in (2), the phase offsets do not affect

Fig. 2. Performance of the CE-OFDM phase demodulator receiver. ($M = 8$, $N_{\text{DFT}} = 512$, oversampling factor $C_{\text{os}} = 4$, $N = 126$ subcarriers)

demodulation [38][1].

The noise component in (6) is

$$N[k] = \frac{1}{T} \int_0^T \xi(t) q_k(t) dt. \qquad (10)$$

The nonlinearity of $\xi(t)$ complicates analysis. Assuming a high carrier-to-noise ratio, $A \gg A_w(t)$, and $\xi(t)$ is well approximated as zero-mean Gaussian noise [51, p. 419], with power density spectrum [48, p. 410]

$$\Phi_{\xi\xi}(f) \approx \frac{N_0}{A^2}, \quad |f| \le W/2. \qquad (11)$$

Approximating $\xi(t)$ as zero mean and Gaussian implies that $N[k]$ is approximated as a zero-mean Gaussian random variable [53]. The variance of $N[k]$ is approximated by observing that (10), due to the fact that $q_k(t)$ is sinusoidal, can be viewed as a Fourier coefficient of $\xi(t)$ [54, pp. 41–43]. Thus [54, p. 43],

$$\text{var}\{N[k]\} \approx \frac{1}{2T} \Phi_{\xi\xi}(f)|_{f=f_k}, \qquad (12)$$

where f_k is the frequency of the kth subcarrier. Since, by definition, $|f_k| \le W/2$, and applying (11), (12) reduces to

$$\text{var}\{N[k]\} \approx \frac{1}{2T} \frac{N_0}{A^2}. \qquad (13)$$

The output of the kth correlator is thus comprised of a PAM signal component $S[k]$ plus an (approximately) additive Gaussian noise component $N[k]$. Determining an approximation to the symbol error rate (SER) for the CE-OFDM system therefore simplifies to the well-known problem of

[1]In order to generate a real-valued OFDM baseband signal, a conjugate symmetric IDFT is used in this paper. Alternatively, an inverse discrete sine transform (IDST) or an inverse discrete cosine transform (IDCT) may be used [11, sec. 3.1], [34], [35], [39]. For these transforms, (9) is not true for all k since the resulting half-cycle sinusoid and cosinusoid subcarriers do not necessarily have an integer number of oscillations over $0 \le t \le T$ [52].

determining the SER for conventional PAM [46, pp. 264–266]. It is straightforward to show that [11, p. 64]

$$\text{SER} \approx 2\left(\frac{M-1}{M}\right) Q\left(2\pi h \sqrt{\frac{6\log_2 M}{M^2-1} \frac{\mathcal{E}_b}{N_0}}\right), \qquad (14)$$

high CNR, where $Q(x) = \int_x^\infty e^{-y^2/2} dy / \sqrt{2\pi}$ is the Gaussian Q-function, and $\mathcal{E}_b = A^2 T/(2N \log_2 M)$ is the energy per bit of the transmitted bandpass CE-OFDM signal, with carrier frequency f_c Hz, $\Re\{s(t)e^{j2\pi f_c t}\}$. Notice that for $2\pi h = 1$, (14) is equivalent to the SER for conventional M-PAM [47, pp. 194–195]. To determine an approximation to the bit error rate, Gray-encoded bit mappings [46, p. 170] are assumed. For high CNR, the only significant symbol errors are those that occur in adjacent signal levels [47, p. 195]. Therefore the BER is [46, p. 271]

$$\begin{aligned} \text{BER} &\approx \frac{\text{SER}}{\log_2 M} \\ &\approx 2\left(\frac{M-1}{M\log_2 M}\right) Q\left(2\pi h \sqrt{\frac{6\log_2 M}{M^2-1} \frac{\mathcal{E}_b}{N_0}}\right), \end{aligned} \qquad (15)$$

high CNR.

To demonstrate the accuracy of (15), an $M = 8$ CE-OFDM system is simulated[2]. The DFT size is $N_{\text{DFT}} = 512$ and an oversampling factor of $C_{\text{os}} = 4$ is used; resulting in $N = N_{\text{DFT}}/C_{\text{os}} - 2 = 512/4 - 2 = 126$ subcarriers. For this baseline AWGN simulation, the equalizer is not required. The phase demodulator performs arctangent calculations on the discrete-time samples $r[n] = s[n]e^{j\phi_0} + w[n]$, then the phase unwrapper is used to avoid phase jumps in the event that the received phase crosses the π-radian boundary. The estimated phase sequence, $\hat{\phi}[n]$, is then processed by the DFT to obtain the demodulated PAM data symbols $Q[k]$,

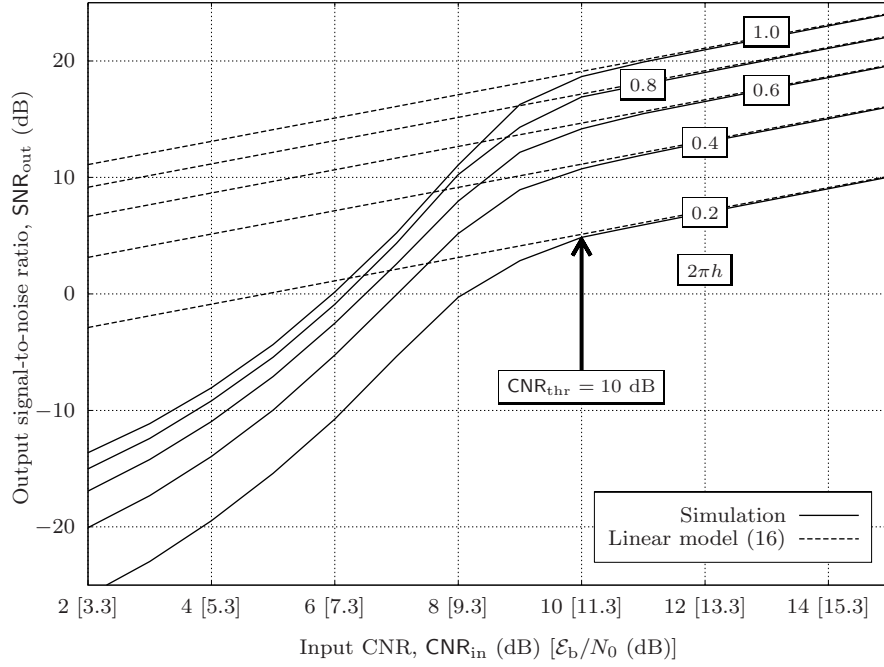[2]See [11] for $M = 2$, $M = 4$, and $M = 16$ simulation results.

Fig. 3.   Threshold effect for various modulation indexes. The system is above threshold when $\text{CNR}_{\text{in}} > \text{CNR}_{\text{thr}} = 10$ dB. ($M = 8$ PAM data symbols, $N_{\text{DFT}} = 512$, oversampling factor $C_{\text{os}} = 4$, $N = 126$ subcarriers)

$k = 1, 2, \ldots, N$. The demodulated PAM data symbols are then used to define the demodulated QAM data symbols $\{\hat{X}[k]\}$ which are processed by the QAM demapper (see Fig. 1).

Figure 2 shows simulation results of the discrete-time CE-OFDM phase demodulator receiver for modulation index values $2\pi h = 0.1, 0.2, \ldots, 0.8, 1.0, 1.3$ and 1.5. The system is simulated with and without channel phase offsets. For both cases, when $2\pi h \leq 1.3$, the BER is shown to be nearly indistinguishable. This verifies the observation made above, from (9), that CE-OFDM is not necessarily impacted by channel phase offsets. Notice that for $2\pi h = 1.0$, CE-OFDM has the same performance as conventional 8-PAM (so long as $\mathcal{E}_{\text{b}}/N_0 > 10$ dB). This confirms the observation made from (14). For $2\pi h > 1.0$, the performance of CE-OFDM can outperform the underlying M-PAM subcarrier modulation. This is analogous to the well-known fact that analog angle modulation can outperform [in terms of the baseband signal-to-noise (SNR) ratio at the output of the demodulator] analog amplitude modulation [48, pp. 413–414]. The price paid is increased spectral occupancy as indicated by (4).

The analytical approximation in (15) is shown to closely match simulation results, given that the modulation index is small and bit energy-to-noise density ratio is high. For the larger modulation index $2\pi h = 1.3$, the analytical expression becomes less accurate; and for $2\pi h = 1.5$, an irreducible error floor develops at BER $= 2 \times 10^{-4}$. This illustrates the limitation of the discrete-time arctangent phase demodulator. Properly phase unwrapping a noisy signal is a difficult problem. Occasional phase jumps at the output of the phase demodulator corrupts $\hat{\phi}[n]$ and degrades BER performance. One simple measure to improve performance is to increase the oversampling factor. For example, it has been observed that an oversampling factor of $C_{\text{os}} = 8$ eliminates the error floor for the $2\pi h = 1.5$ case [11, p. 81]. However, this also

increases complexity for a given data rate.

It is evident from the results in Fig. 2 that (15) acts as a lower bound on the BER. This is explained as follows. The key assumption made to obtain (15) is high CNR which, in effect, linearizes the phase demodulator. With this assumption, the input to the correlator bank simplifies to the transmitted message signal $m(t)$ plus additive Gaussian noise, which appears frequency-flat over the signal bandwidth as indicated by (11). Thus, the correlator bank (implemented with the DFT) is the optimum demodulator [46, pp. 242–247], and the SER and BER are expressed by (14) and (15) respectively. For low CNR, nonlinearities cause the correlator bank to be sub-optimum and BER performance is necessarily worse than (15).

At low CNR, the system is said to be below threshold [48, pp. 414–417]. For conventional analog angle modulated systems, a commonly accepted theshold CNR is $\text{CNR}_{\text{thr}} = 10$ dB [44, pp. 120–138], [45]. As shown by the results in Fig. 3, this threshold CNR applies to the CE-OFDM phase demodulator receiver studied in this paper. The x-axis represents the CNR at the input to the phase demodulator[3]:

$$\text{CNR}_{\text{in}} \equiv \frac{\text{Power of } \Re\{s(t)e^{j2\pi f_c t}\}}{\text{Power of } \Re\{w(t)e^{j2\pi f_c t}\}} = \frac{A^2/2}{N_0 B_{\text{bpf}}},$$

where B_{bpf} is the bandwidth of the front-end bandpass filter. For these results, $B_{\text{bpf}} = F_0$ (resulting in uncorrelated noise samples $\{w[n]\}$ [11, p. 62]). The y-axis represents the SNR at the output of the correlator bank, defined as $\text{SNR}_{\text{out}} \equiv \text{E}\{\text{SNR}_{\text{out}}[k]\}$, where $\text{E}\{\cdot\}$ is the expectation operator, and $\text{SNR}_{\text{out}}[k] \equiv S^2[k]/\text{var}\{N[k]\}$ is the SNR at the output of the kth correlator. Invoking the high CNR assumption, it is straightforward to show that

$$\text{SNR}_{\text{out}} \approx C \cdot \text{CNR}_{\text{in}}, \qquad (16)$$

[3]The x-axis is also labeled with the bit energy-to-noise density ratio, which is related to the input CNR as $\mathcal{E}_{\text{b}}/N_0 = \text{CNR}_{\text{in}} \cdot N_{\text{DFT}}/(N \log_2 M)$.
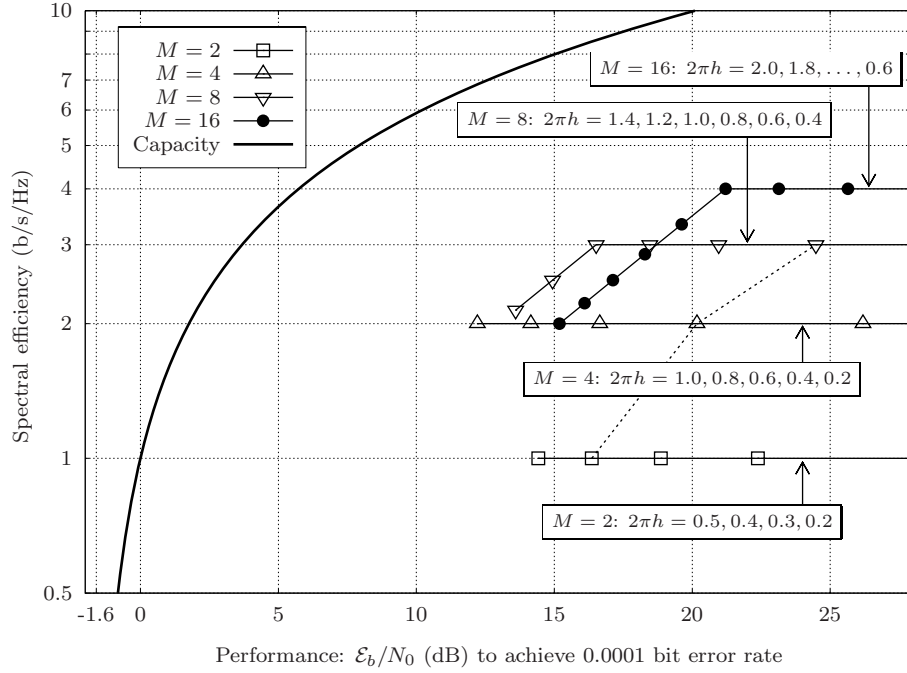
Fig. 4. Spectral efficiency versus performance.

where $C = (2\pi h)^2 \cdot 2N_{\mathrm{DFT}}/N$. The results in Fig. 3 show that the output SNR matches the linear model for input CNR above 10 dB. Below 10 dB, the system drops below threshold.

This problem can be alleviated with threshold extension techniques [45]. Most notably, phase locked loops are known to reduce the threshold in FM systems by several dB. In [55], for example, the threshold CNR is reduced from 10 dB to 0 dB. Therefore replacing the simple $\arg(\cdot)$ phase demodulator with a more sophisticated structure such as a phase locked loop can potentially improve CE-OFDM performance at low $\mathcal{E}_{\mathrm{b}}/N_0$.

Figure 4 plots the spectral efficiency, expressed by (4), versus the required $\mathcal{E}_{\mathrm{b}}/N_0$ to achieve a BER of 1e-4. For each M, the modulation index values plotted have been observed to closely match (15), at the target BER, for a CE-OFDM system with $C_{\mathrm{os}} = 8$ in conjunction with a finite impulse response (FIR) lowpass filter[4] preceding the arctangent calculator [38]. For fixed modulation index values, CE-OFDM has improved spectral efficiency with increased modulation order M at the cost of performance degradation. For example, consider $2\pi h = 0.4$ (see dash line in the figure). The spectral efficiency is 1, 2 and 3 b/s/Hz for $M = 2, 4$ and 8, respectively. The required $\mathcal{E}_{\mathrm{b}}/N_0$ is 4 dB greater for $M = 4$ than for $M = 2$, 4.5 dB greater for $M = 8$ than for $M = 4$. This type of spectral efficiency/performance tradeoff is the same for common linear modulations such as M-PAM, M-PSK and M-QAM [46, p. 282]. By varying the modulation index, however, CE-OFDM can have both improvements in spectral efficiency and in performance. For example, the $M = 4$, $2\pi h = 1.0$ modulation has twice the spectral efficiency as the $M = 2$, $2\pi h = 0.5$ case, while at the same time requiring 2 dB less $\mathcal{E}_{\mathrm{b}}/N_0$ to

achieve the target BER. Other nonlinear modulation formats such as conventional continuous-phase modulation (CPM) also have the potential for simultaneous spectral efficiency and performance gains [56]. For conventional CPM, however, this gain generally comes with the cost of increased receiver complexity due to phase trellis decoding. For CE-OFDM, as with conventional OFDM, the receiver complexity is due mainly to the DFT and not greatly influenced by the modulation order of the data symbols M.

IV. PERFORMANCE OVER FADING CHANNELS

Performance analysis is now extended to the case of fading channels. In Section IV-A, performance bounds are derived for CE-OFDM in Rayleigh and Ricean frequency-nonselective fading channels. Section IV-B then considers the performance of CE-OFDM in frequency-selective fading channels.

A. Frequency-Nonselective Fading Channels

In the case of flat fading, the received signal is represented as $r(t) = \alpha s(t)e^{j\phi_0} + w(t)$. For a given channel amplitude α, the bit energy-to-noise density ratio is $\gamma = \alpha^2 \mathcal{E}_{\mathrm{b}}/N_0$, and the average bit energy-to-noise density ratio is [46, p. 817] $\bar{\gamma} = \mathsf{E}\{\gamma\} = \mathsf{E}\left\{\alpha^2\right\} \mathcal{E}_{\mathrm{b}}/N_0$. It is desired to calculate the bit error rate at a given $\bar{\gamma}$, denoted as $\mathsf{BER}(\bar{\gamma})$. This quantity depends on the statistical distribution of γ. For channels with a line-of-sight (LOS) component, the probability density function of γ is modeled as [47, p. 102]

$$
p_\gamma(x) = \frac{(1 + K_{\mathrm{Rice}})e^{-K_{\mathrm{Rice}}}}{\bar{\gamma}} \exp\left[-\frac{(1 + K_{\mathrm{Rice}})x}{\bar{\gamma}}\right]
$$
$$
I_0\left[2\sqrt{\frac{K_{\mathrm{Rice}}(1 + K_{\mathrm{Rice}})x}{\bar{\gamma}}}\right], \tag{17}
$$

$x \geq 0$, where $I_0(\cdot)$ is the 0th-order modified Bessel function of the first kind, and $K_{\mathrm{Rice}} = \rho^2/2\sigma_0^2$ is the Rice factor: ρ^2 and

[4]The FIR lowpass filter is designed using the windowing method [50, pp. 623–630] with a Hamming window, 11 taps and a cut-off frequency of 0.2 cycles per sample [38], [11, sec. 4.1.4].

$2\sigma_0^2$ represent the power of the LOS and scatter component, respectively [49, p. 40]. For channels without line-of-sight, $\rho \to 0$ and γ becomes Rayleigh distributed [47, p. 101]:

$$p_\gamma(x) = \frac{1}{\bar{\gamma}} \exp\left(-\frac{x}{\bar{\gamma}}\right), \quad x \geq 0. \tag{18}$$

To obtain $\text{BER}(\bar{\gamma})$, the conditional BER is averaged over the distribution of γ [46, p. 817]:

$$\text{BER}(\bar{\gamma}) = \int_0^\infty \text{BER}(x) p_\gamma(x) dx. \tag{19}$$

As discussed above, the phase demodulator complicates analysis due to the threshold effect. At high CNR, (15) provides an accurate expression for the conditional BER. An approximate lower bound on (19) is therefore obtained by assuming that (15) is accurate for all CNR. In other words, ignoring the threshold effect and assuming that the conditional BER is $\text{BER}(x) = c_1 Q(c_2 \sqrt{x})$, for all $x \geq 0$, where $c_1 = 2(M-1)/(M \log_2 M)$ and $c_2 = 2\pi h \sqrt{6 \log_2 M/(M^2-1)}$, (19) is approximately bounded as

$$\text{BER}(\bar{\gamma}) \geq \int_0^\infty c_1 Q\left(c_2 \sqrt{x}\right) p_\gamma(x) dx \equiv \text{BER}_{\text{LB}}(\bar{\gamma}).$$

Expressions are readily available for $\text{BER}_{\text{LB}}(\bar{\gamma})$. For the Ricean channel [47, p. 102],

$$\text{BER}_{\text{LB, Rice}}(\bar{\gamma}) = \frac{c_1}{\pi} \int_0^{\pi/2} \frac{(1+K_{\text{Rice}})\sin^2\theta}{(1+K_{\text{Rice}})\sin^2\theta + c_2^2\bar{\gamma}/2} \times$$
$$\exp\left[-\frac{K_{\text{Rice}} c_2^2 \bar{\gamma}/2}{(1+K_{\text{Rice}})\sin^2\theta + c_2^2\bar{\gamma}/2}\right] d\theta, \tag{20}$$

which can be computed numerically. For the Rayleigh channel, the lower bound approximation is expressed as [47, p. 101]

$$\text{BER}_{\text{LB, Ray}}(\bar{\gamma}) = \frac{c_1}{2}\left(1 - \sqrt{\frac{c_2^2\bar{\gamma}/2}{1+c_2^2\bar{\gamma}/2}}\right). \tag{21}$$

An upper bound for (19) is obtained by first breaking the integral into $n+1$ regions:

$$\text{BER}(\bar{\gamma}) = \int_0^\infty \text{BER}(x) p_\gamma(x) dx$$
$$= \left[\sum_{i=0}^{n-1} \int_{\gamma_i}^{\gamma_{i+1}} \text{BER}(x) p_\gamma(x) dx\right] \tag{22}$$
$$+ \int_{\gamma_n}^\infty \text{BER}(x) p_\gamma(x) dx,$$

where $\gamma_0 = 0$ and $\gamma_i > \gamma_{i-1}$, $i = 1, 2, \ldots, n$. Since the conditional bit error rate is a monotonically decreasing function [$\text{BER}(x) \leq \text{BER}(\gamma_i)$, $\gamma_i \leq x \leq \gamma_{i+1}$, for $i = 0, 1, \ldots, n-1$], (22) can be upper bounded as

$$\text{BER}(\bar{\gamma}) \leq \left[\sum_{i=0}^{n-1} \text{BER}(\gamma_i) \int_{\gamma_i}^{\gamma_{i+1}} p_\gamma(x) dx\right]$$
$$+ \int_{\gamma_n}^\infty \text{BER}(x) p_\gamma(x) dx \equiv \text{BER}_{\text{UB}}(\bar{\gamma}).$$

This upper bound can be approximated by invoking (15) for the conditional BER in the range $x \geq \gamma_n$:

$$\text{BER}_{\text{UB}}(\bar{\gamma}) \approx \left[\sum_{i=0}^{n-1} \text{BER}(\gamma_i) \int_{\gamma_i}^{\gamma_{i+1}} p_\gamma(x) dx\right]$$
$$+ \int_{\gamma_n}^\infty c_1 Q(c_2\sqrt{x}) p_\gamma(x) dx \tag{23}$$

The conditional BER in the low-CNR range $0 \leq x < \gamma_n$ is difficult to obtain, again, due to the threshold effect. Alternatively, estimating $\{\text{BER}(\gamma_i)\}_{i=1}^{n-1}$ by means of computer simulation is a relatively simple task. This leads to a two-step semi-analytical approach for obtaining an approximation to $\text{BER}_{\text{UB}}(\bar{\gamma})$: 1) estimate $\{\text{BER}(\gamma_i)\}_{i=1}^{n-1}$ with computer simulation [$\text{BER}(\gamma_0) = 0.5$], then 2) compute the $n+1$ integrals in (23) numerically.

Figure 5 compares simulation results with (20), (21) and $\text{BER}_{\text{UB}}(\bar{\gamma})$ as approximated by (23). The semi-analytical approach for calculating (23) is performed as follows. γ_1 is set to 0 dB, then $\text{BER}(\gamma_1)$ is estimated. This process continues for each $\gamma_i = i - 1$ dB, $i = 2, 3, \ldots, n-1$, and stops when the estimated conditional BER is $\text{BER}(\gamma_{n-1}) < 0.01$. This stopping point is chosen since, as demonstrated in Fig. 2, (15) is accurate for $2\pi h \leq 1.0$ and BER ≤ 0.01. γ_n is then set to $n - 1$ dB and (23) is computed using numerical integration. Figure 5(a) shows results for CE-OFDM with modulation index values $2\pi h = 0.2$ and 1.0 in Rayleigh flat fading. For the $2\pi h = 0.2$ case, the lower bound (21) is shown to closely match simulation results for BER $<$ 0.1. At high CNR, and small modulation index, the phase demodulator provides reliable operation. At low CNR, the phase demodulator operates below threshold and the lower bound in (21) is no longer tight. Notice that the upper bound, as approximated by (23), closely matches simulation results at all values of $\bar{\gamma}$. This is also true for the $2\pi h = 1.0$ case. The lower bound becomes less accurate for large modulation index due to phase wrapping problem associated with the phase demodulator. Figure 5(b) shows results for CE-OFDM with modulation index values $2\pi h = 0.2$, 0.5 and 1.2 in a Ricean channel with Rice factor $K_{\text{Rice}} = 10$ dB. Like the lower bound for the Rayleigh case, (20) is shown to be accurate for small modulation index and high CNR. For the large modulation index case $2\pi h = 1.2$, at BER ≤ 0.01, (20) is shown to be overly optimistic by 2 dB. The approximation to $\text{BER}_{\text{UB}}(\bar{\gamma})$ is shown to provide a tight upper bound for each $2\pi h$ at all displayed $\bar{\gamma}$.

These results demonstrate the usefulness, and limitations, of (20) and (21). By ignoring the threshold effect, and making use of the high-CNR approximation (15), these simple expressions are obtained. For high $\bar{\gamma}$ and small modulation index, (20) and (21) are shown to provide tight lower bounds. However, at low $\bar{\gamma}$ these expressions are less accurate. The approximation to the upper bound (23) [and the procedure described to obtain it] is shown to provide curves that closely match simulation results. The limitation of (23) is the required computer simulation to estimate the conditional BERs in the below-threshold region, $\{\text{BER}(\gamma_i)\}_{i=1}^{n-1}$.
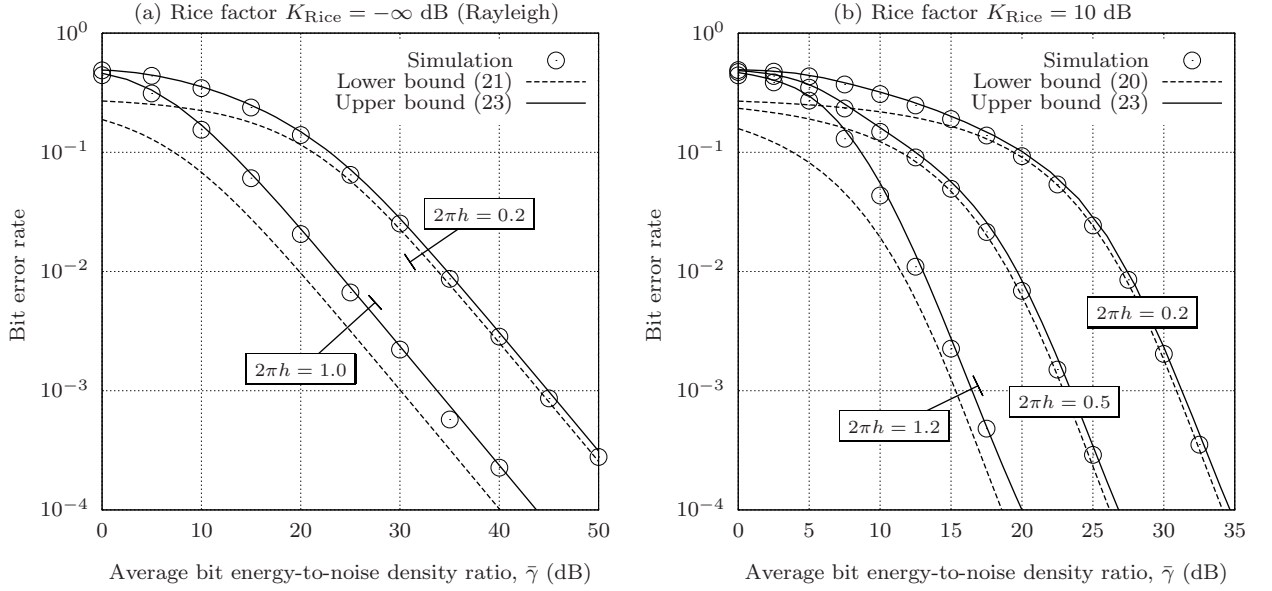
Fig. 5. Performance of CE-OFDM in flat fading channels. ($M = 8$ PAM data symbols, $N_{\mathrm{DFT}} = 512$, oversampling factor $C_{\mathrm{os}} = 4$, $N = 126$ subcarriers)

B. Frequency-Selective Fading Channels

In this section it will be shown that with proper equalization CE-OFDM achieves reliable operation over multipath fading channels. Equalization is simplified with the cyclic prefix transmission used in conventional OFDM. As shown by (5), the effect of the channel simplifies to an IDFT, followed by a vector multiplication, followed by a DFT. The frequency-domain equalizer has this same structure. Defined by $\{C[k]\}$, the FDE attempts to correct the distortion caused by the channel, defined by $\{H[k]\}$. For the zero-forcing (ZF) definition,

$$C[k] = \frac{1}{H[k]},$$

$k = 0, 1, \ldots, N_{\mathrm{DFT}} - 1$, while the minimum mean-squared error (MMSE) equalizer definition is

$$C[k] = \frac{H^*[k]}{|H[k]|^2 + (\mathcal{E}_{\mathrm{b}}/N_0)^{-1}},$$

$k = 0, 1, \ldots, N_{\mathrm{DFT}} - 1$ [57]. The output of the equalizer is $\hat{s}[n] = \mathsf{DFT}^{-1}\{R[k]C[k]\} = r[n] \circledast c[n]$, $n = 0, \ldots, N_{\mathrm{DFT}} - 1$, where $r[n]$ and $R[k]$ are DFT pairs, and $c[n]$ and $C[k]$ are DFT pairs. In the absence of noise, the MMSE and ZF definitions are equivalent and $\hat{s}[n] = \mathsf{DFT}^{-1}\{S[k]H[k]/H[k]\} = s[n]$. The DFTs in the FDE are implemented with FFTs having complexity $O(0.5N_{\mathrm{DFT}} \log_2 N_{\mathrm{DFT}})$ [50, p. 459].

Computer simulation is used to evaluate the effectiveness of the FDE. Time-invariant frequency-selective fading channel models, characterized by the statistics of the channel taps $\{h[l]\}$, are considered. For each model, the channel taps are zero mean, complex valued and Gaussian distributed, resulting in Rayleigh fading [49]. The channel is normalized such that $\sum_{l=0}^{L-1} \mathsf{E}\{|h[l]|^2\} = 1$. Channels A and B are two-path models having a secondary path delayed 5 μs [6]: A has a weak secondary path (one-tenth the power of the primary path); B has a strong secondary path (one-half the power of the primary path). Channel C has an exponential power delay

profile[5] where $\mathsf{E}\{|h[l]|^2\} \propto \exp(-\tau_l/2\mu\mathrm{s})$, $0 \le \tau_l \le 8.75$ μs. Channel D has a uniform power delay profile where $\mathsf{E}\{|h[l]|^2\} = 1/36$, $0 \le \tau[l] \le 8.75$ μs. The sampling rate is $F_0 = 4\mathrm{e}6$ samp/sec, the DFT size is $N_{\mathrm{DFT}} = 512$, and the block period is $T = 128$ μs. An $N_{\mathrm{cp}} = 40$-sample, $T_{\mathrm{cp}} = 10$ μs cyclic prefix is used, resulting in a transmission efficiency of $\eta = 128\mu\mathrm{s}/(128\mu\mathrm{s} + 10\mu\mathrm{s}) \approx 0.93$. The oversampling factor is $C_{\mathrm{os}} = 8$, the number of subcarriers is $N = 62$ and the bandwidth of the message signal is $W = 484.375$ kHz.

The simulation results, shown in Fig. 6, show that uncoded CE-OFDM exploits multipath diversity. For $2\pi h = 1.0$, channel D with MMSE equalization outperforms the flat fading result by 12 dB. Notice the progressive improvement in performance from channel A to channel D. This is due to the increased multipath diversity: for channel A, over 90% of the channel gain depends on a single path, while channel D has, on average, equal contribution from each of its 36 paths. The fact that uncoded CE-OFDM exploits multipath diversity is interesting since uncoded OFDM does not [11, sec. 1.1.2], [58]. The diversity gain in CE-OFDM is explained by viewing the Taylor series expansion [59, p. 146] of the transmitted signal ($\theta = 0$):

$$s(t) = Ae^{j\phi(t)} = A\left[1 + j\sigma_\phi m(t) - \frac{\sigma_\phi^2}{2!}m^2(t) - j\frac{\sigma_\phi^3}{3!}m^3(t) + \ldots\right], \quad (24)$$

$\sigma_\phi = 2\pi h$. The higher-order terms, $\{m^n(t)\}_{n\ge 2}$, result in an n-fold convolution in the frequency domain representation of the message signal, and thus spreading of the data symbols $\{I[k]\}$. This frequency-domain spreading results in improved performance in frequency-selective fading channels.

Also shown in Fig. 6 are results for the small modulation index case $2\pi h = 0.1$. For small modulation index values, CE-OFDM does not achieve multipath diversity since the first

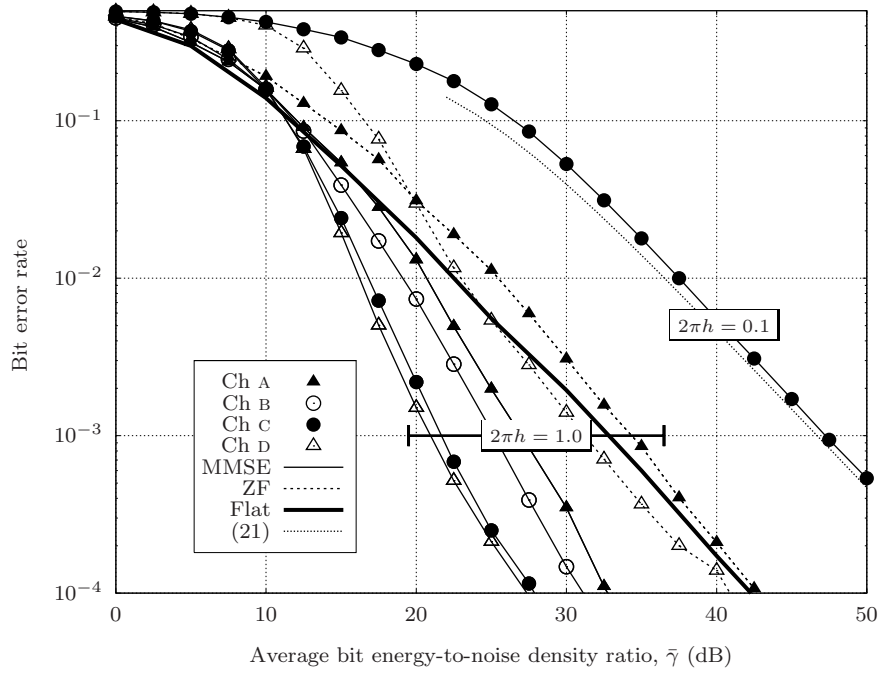[5]These channel models are studied in detail in [11, sec. 6.2].

Fig. 6. Performance of CE-OFDM in Rayleigh fading channels. ($M = 4$, $N_{DFT} = 512$, oversampling factor $C_{os} = 8$, $N = 62$ subcarriers)
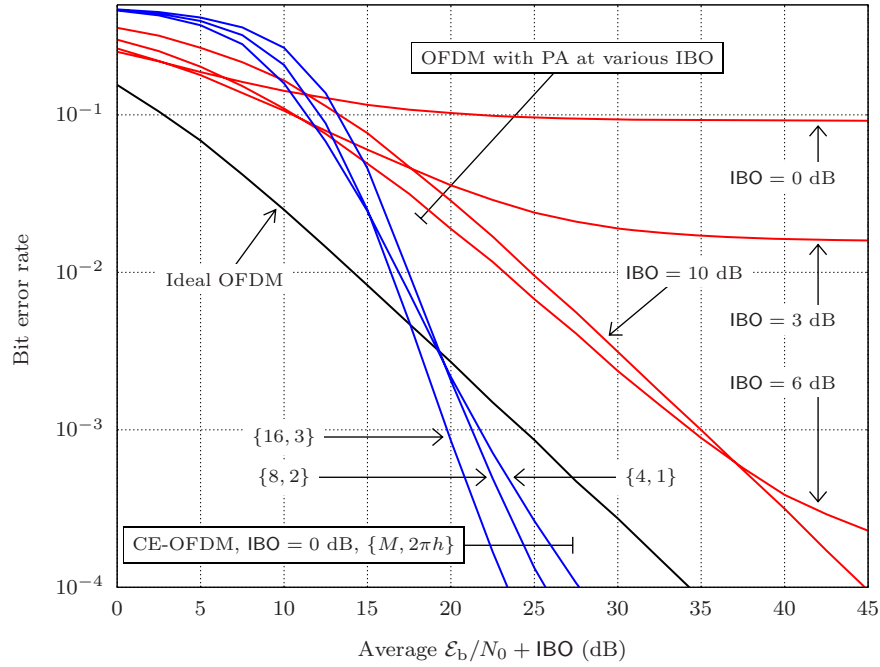

Fig. 7. CE-OFDM versus QPSK OFDM. (Channel model C, $N = 62$ subcarriers, MMSE FDE)

two terms in (24) dominate, $s \approx A[1 + j\sigma_\phi m(t)]$. In this case, (21) provides a lower bound for both single-path and multipath fading.

Finally, notice the performance gain had by using MMSE versus ZF equalization. ZF noise enhancement [46, p. 621] is particularly problematic at low SNR.

V. A COMPARISON BETWEEN CONSTANT ENVELOPE AND CONVENTIONAL OFDM

In this section CE-OFDM is compared to QPSK OFDM in the presence of power amplifier nonlinearities. The PA is modeled as an instantaneous nonlinearity [60, chap. 5], having input

$$s_{in}(t) = \mathcal{A}_{in}(t) \exp[j\phi_{in}(t)]$$

and output

$$s_{out}(t) = G[\mathcal{A}_{in}(t)] \exp[j\{\phi_{in}(t) + \Phi[\mathcal{A}_{in}(t)]\}],$$

where G and Φ are respectively the AM/AM and AM/PM conversions of the amplifier model. In this comparison, the Saleh model is used [14], [61], [11, p. 27]:

$$G[\mathcal{A}_{in}(t)] = \frac{g_0 \mathcal{A}_{in}(t)}{1 + [\mathcal{A}_{in}(t)/\mathcal{A}_{sat,in}]^2},$$
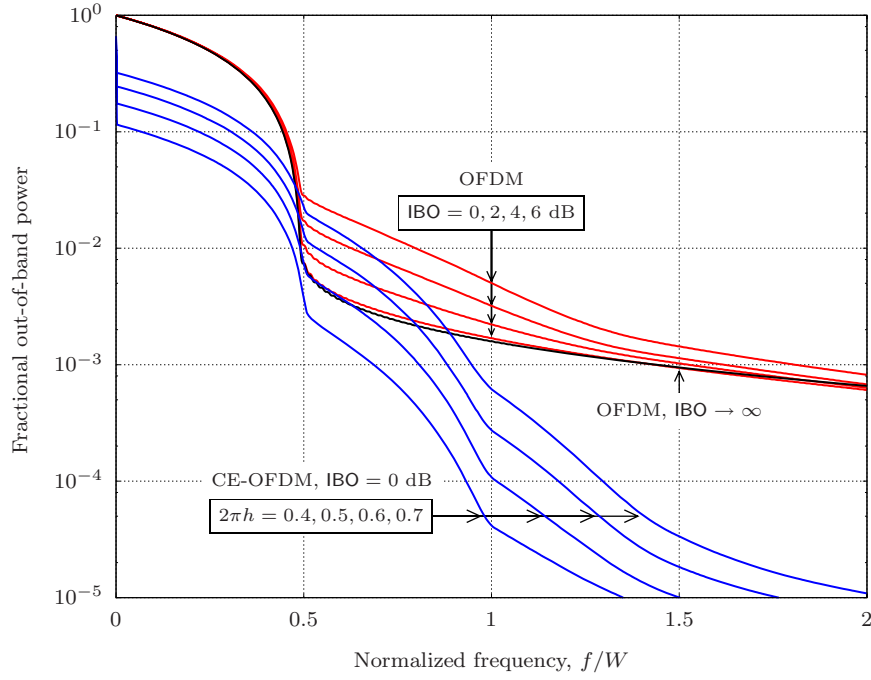
Fig. 8. CE-OFDM versus OFDM with nonlinear power amplification. ($N = 62$ subcarriers)

and

$$\Phi\left[\mathcal{A}_{\text{in}}(t)\right] = \frac{\alpha_\phi \mathcal{A}_{\text{in}}^2(t)}{1 + \beta_\phi \mathcal{A}_{\text{in}}^2(t)}.$$

This model is characterized by the gain g_0, the input saturation amplitude $\mathcal{A}_{\text{sat,in}}$, and the AM/PM parameters α_ϕ and β_ϕ. For the results in this paper, $\alpha_\phi = \pi/12$ and $\beta_\phi = 1/4$ [14]. The PA nonlinearity is determined by the PAPR of the input signal [62] and by the input power backoff, defined as [63]

$$\text{IBO} \equiv \frac{\mathcal{A}_{\text{sat,in}}^2}{\mathsf{E}\left\{\mathcal{A}_{\text{in}}^2(t)\right\}} \geq 1.$$

For CE-OFDM, $\mathcal{A}_{\text{in}}(t) = A$, the PAPR is 0 dB, and nonlinear distortion is avoided. CE-OFDM operates at $\text{IBO} = 0$ dB, maximizing the range and the efficiency of the PA [17]. For OFDM, $\mathcal{A}_{\text{in}}(t)$ is Rayleigh distributed [9] resulting in a large PAPR. To avoid nonlinear distortion, large backoff is required, reducing range and PA efficiency [17], [64].

Figure 7 shows simulation results for channel model C. The x-axis is adjusted to account for the negative impact of input power backoff [57]. Three CE-OFDM systems are shown: $M = 4$, $2\pi h = 1$; $M = 8$, $2\pi h = 2$; and $M = 16$, $2\pi h = 3$. The advantage of CE-OFDM is demonstrated in this figure. At high average $\mathcal{E}_{\text{b}}/N_0$, CE-OFDM provides significant performance improvement due primarily to the 0 dB backoff. The OFDM system with 0 dB IBO has an error floor at the bit error rate 0.1. At the bit error rate 0.001, the IBO that results in the best OFDM performance is 6 dB, where $\mathcal{E}_{\text{b}}/N_0 + \text{IBO} = 34$ dB. The CE-OFDM system achieves this target bit error rate with a 12–15 dB gain over the OFDM system. Moreover, since $\text{IBO} = 0$ dB, the PA efficiency is maximized for CE-OFDM.

The CE-OFDM system also achieves frequency diversity. In fact, for BER < 0.002, the CE-OFDM system outperforms the ideal OFDM system, amplified with an ideal linear PA, which has Rayleigh flat fading QPSK performance [46, p. 831].

The CE-OFDM curves in Fig. 7 demonstrate the observation made from Fig. 4, that performance can improve with increased M so long as the modulation index increases as well. The $M = 16$, $2\pi h = 3$ system outperforms the $M = 4$, $2\pi h = 1$ system by nearly 5 dB at the BER 0.0001. However, as (3) indicates, the signal bandwidth grows with $2\pi h$, which in turn reduces spectral efficiency expressed by (4). Of the three CE-OFDM systems, $M = 4$, $2\pi h = 1$ results in the highest spectral efficiency (2 b/s/Hz) followed by $M = 8$, $2\pi h = 2$ (1.5 b/s/Hz) and $M = 16$, $2\pi h = 3$ (1.33 b/s/Hz). To achieve 4 b/s/Hz, $M_{\text{PAM}} = 16$, $2\pi h = 1$ can be used, at the cost of degraded performance. Thus the trade between spectral efficiency and performance is made with the two parameters M and $2\pi h$. For the QPSK OFDM system, the spectral efficiency is 2 b/s/Hz, given that spectral broadening caused by the PA is avoided.

Figure 8 compares fractional out-of-band power curves for conventional OFDM [11, sec. 1.1.2] and CE-OFDM. CE-OFDM operates with 0 dB backoff and the fractional out-of-band power depends only on the modulation index. Conventional OFDM is sensitive to the PA, requiring large backoff to avoid spectral broadening. At $\text{IBO} = 0$ dB, the CE-OFDM curves, for each modulation index $2\pi h = 0.4, 0.5, 0.6$, and 0.7, are shown to be lower than the OFDM curves at the same backoff level. In the range $0.5 < f/W < 0.8$, OFDM can have better containment than CE-OFDM, but only for increased levels of backoff and, therefore, lower PA efficiency. Due to CE-OFDM's phase-continuous design [37], it exhibits faster sidelobe rolloff than conventional OFDM.

An implementation of the CE-OFDM waveform was developed on a small-form-factor software defined radio (SDR) utilizing a Xilinx Virtex 4 field programmable gate array (FPGA) and a Texas Instruments OMAP 5912, which is an integrated microprocessor consisting of an ARM9 host

(a) OFDM mode. (High PAPR)
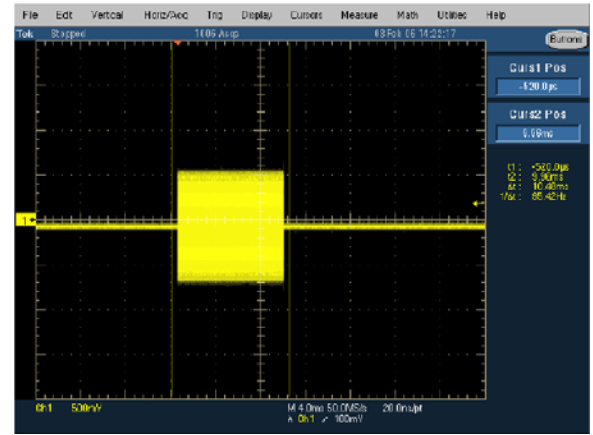
(b) CE-OFDM mode. (0 dB PAPR)

Fig. 9.   Oscilloscope capture of OFDM/CE-OFDM software defined radio implementation.

processor and a C55x digital signal processor (DSP) [65], [66]. The FPGA is used for high rate processing (such as digital down conversion from IF to baseband), while the DSP performs all other physical layer processing. The ARM9 host processor runs embedded Linux and handles all link layer and networking tasks. CE-OFDM was implemented by adding the required additional operations (see Fig. 1) to an existing OFDM implementation. All waveform processing was performed on the C55x DSP using a 16-bit fixed point implementation. Figure 9 shows the time series at the 10.7 MHz IF output. The OFDM signal exhibits a high PAPR [Fig. 9(a)] while the CE-OFDM signal has the desirable constant envelope property [Fig. 9(b)].

VI. CONCLUSION

In this paper a transformation technique that eliminates the PAPR problem associated OFDM is developed. The phase modulation transform results in 0 dB PAPR constant envelope signals ideally suited for nonlinear, efficient amplification. CE-OFDM is studied over a wide range of channel conditions. An analytical approximation to the AWGN BER performance is derived. This approximation is used to derive performance lower bounds for Rayleigh and Ricean flat fading. For frequency-selective fading channels, a frequency-domain equalizer is proposed. Like conventional OFDM, cyclic prefix transmission is used to simplify equalization. It is demonstrated that uncoded CE-OFDM exploits multipath diversity. CE-OFDM is shown to compare favorably to conventional OFDM in multipath fading channels when the impact of nonlinear power amplification is taken into account. CE-OFDM is also shown to suffer from the FM threshold effect, however. Potential solutions to this problem, including threshold extension with phase locked loops, are discussed.

ACKNOWLEDGMENTS

Thanks to Prof. Milstein (University of California, San Diego), Prof. Pettit (California State University, Northridge), and Drs. North and Axford (SPAWAR Systems Center, San Diego) for the many helpful technical discussions; Chris Vander Valk and Marc Lerch (Nova Engineering, Cincinnati,

Ohio) for their implementation expertise; and the anonymous reviewers for improving the quality of this paper.

REFERENCES

[1] R. W. Chang, "Synthesis of band-limited orthogonal signals for multichannel data transmission," *Bell Syst. Tech. J.*, vol. 45, pp. 1775–1796, Dec. 1966.

[2] S. B. Weinstein and P. M. Ebert, "Data transmission by frequency-division multiplexing using the discrete Fourier transform," *IEEE Trans. Commun. Technol.*, vol. 19, no. 5, pp. 628–634, Oct. 1971.

[3] L. J. Cimini, Jr., "Analysis and simulation of a digital mobile channel using orthogonal frequency division multiplexing," *IEEE Trans. Commun.*, vol. 33, no. 7, pp. 665–675, July 1985.

[4] W. Y. Zou and Y. Wu, "COFDM: an overview," *IEEE Trans. Broadcast.*, vol. 41, no. 1, pp. 1–8, Mar. 1995.

[5] R. van Nee, G. Awater, M. Morikura, H. Takanashi, M. Webster, and K. W. Halford, "New high-rate wireless LAN standards," *IEEE Commun. Mag.*, pp. 82–88, Dec. 1999.

[6] P. H. Moose, D. Roderick, R. North, and M. Geile, "A COFDM-based radio for HDR LOS networked communications," in *Proc. IEEE ICC*, vol. 1, June 1999, pp. 187–192.

[7] I. Koffman and V. Roman, "Broadband wireless access solutions based on OFDM access in IEEE 802.16," *IEEE Commun. Mag.*, pp. 96–103, Apr. 2002.

[8] H. Yang, "A road to future broadband wireless access: MIMO-OFDM-based air interface," *IEEE Commun. Mag.*, pp. 53–60, Jan. 2005.

[9] S. Shepherd, J. Orriss, and S. Barton, "Asymptotic limits in peak envelope power reduction by redundant coding in orthogonal frequency-division multiplex modulation," *IEEE Trans. Commun.*, vol. 46, no. 1, pp. 5–10, Jan. 1998.

[10] H. Ochiai and H. Imai, "On the distribution of the peak-to-average power ratio in OFDM signals," *IEEE Trans. Commun.*, vol. 49, no. 2, pp. 282–289, Feb. 2001.

[11] S. C. Thompson, "Constant envelope OFDM phase modulation," Ph.D. dissertation, University of California, San Diego, 2005. [Online]. Available: http://elsteve.com/thesis/

[12] P. Banelli, "Theoretical analysis and performance of OFDM signals in nonlinear fading channels," *IEEE Trans. Wireless Commun.*, vol. 2, no. 2, pp. 284–293, Mar. 2003.

[13] G. Cariolaro, G. Michieletto, G. Stivanello, and L. Vangelista, "Spectral analysis at the output of a TWT driven by an OFDM signal," in *Proc. ICCS*, vol. 2, Singapore, Nov. 1994, pp. 653–657.

[14] E. Costa, M. Midrio, and S. Pupolin, "Impact of amplifier nonlinearities on OFDM transmission system performance," *IEEE Commun. Lett.*, vol. 3, no. 2, pp. 37–39, Feb. 1999.

[15] D. Dardari, V. Tralli, and A. Vaccari, "A theoretical characterization of nonlinear distortion effects in OFDM systems," *IEEE Trans. Commun.*, vol. 48, no. 10, pp. 1755–1764, Oct. 2000.

[16] P. Banelli, G. Baruffa, and S. Cacopardi, "Effects of HPA non linearity on frequency multiplexed OFDM signals," *IEEE Trans. Broadcast.*, vol. 47, no. 2, pp. 123–136, June 2001.

[17] F. H. Raab, P. Asbeck, S. Cripps, P. B. Kenington, Z. B. Popovic, N. Pothecary, J. F. Sevic, and N. O. Sokal, "Power amplifiers and transmitters for RF and microwave," *IEEE Trans. Microwave Theory Tech.*, vol. 50, no. 3, pp. 814–826, Mar. 2002.

[18] S. L. Miller and R. J. O'Dea, "Peak power and bandwidth efficient linear modulation," *IEEE Trans. Commun.*, vol. 46, no. 12, pp. 1639–1648, Dec. 1998.

[19] H. Ochiai, "Power efficiency comparison of OFDM and single-carrier signals," in *Proc. IEEE VTC*, vol. 2, Sept. 2002, pp. 899–903.

[20] D. Wulich, "Definition of efficient PAPR in OFDM," *IEEE Commun. Lett.*, vol. 9, no. 9, pp. 832–834, Sept. 2005.

[21] M. Kiviranta, A. Mämmelä, D. Cabric, D. A. Sobel, and R. W. Brodersen, "Constant envelope multicarrier modulation: performance evaluation in AWGN and fading channels," in *Proc. IEEE Milcom*, vol. 2, Oct. 2005, pp. 807–813.

[22] A. R. S. Bahai, M. Singh, A. J. Goldsmith, and B. R. Saltzberg, "A new approach for evaluating clipping distortion in multicarrier systems," *IEEE J. Select. Areas Commun.*, vol. 20, no. 5, pp. 1037–1046, June 2002.

[23] S. Sezginer and H. Sari, "OFDM peak power reduction with simple amplitude predistortion," *IEEE Commun. Lett.*, vol. 10, no. 2, pp. 65–67, Feb. 2006.

[24] J. A. Davis and J. Jedwab, "Peak-to-mean power control in OFDM, Golay complementary sequences, and Reed-Muller codes," *IEEE Trans. Inform. Theory*, vol. 45, no. 7, pp. 2397–2417, Nov. 1999.

[25] B. S. Krongold and D. L. Jones, "An active-set approach for OFDM PAR reduction via tone reservation," *IEEE Trans. Signal Processing*, vol. 52, no. 2, pp. 495–509, Feb. 2004.

[26] A. D. S. Jayalath and C. R. N. Athaudage, "On the PAR reduction of OFDM signals using multiple signal representation," *IEEE Commun. Lett.*, vol. 8, no. 7, pp. 425–427, July 2004.

[27] M. Pauli and H.-P. Kuchenbecker, "Minimization of the intermodulation distortion of a nonlinearly amplified OFDM signal," *Wireless Personal Commun.*, vol. 4, no. 1, pp. 93–101, Jan. 1996.

[28] J. Armstrong, "Peak-to-average power reduction for OFDM by repeated clipping and frequency domain filtering," *IEE Electron. Lett.*, vol. 38, no. 5, pp. 246–247, Feb. 2002.

[29] A. N. D'Andrea, V. Lottici, and R. Reggiannini, "Nonlinear predistortion of OFDM signals over frequency-selective fading channels," *IEEE Trans. Commun.*, vol. 49, no. 5, pp. 837–843, May 2001.

[30] J. Tellado, L. M. C. Hoo, and J. M. Cioffi, "Maximum-likelihood detection of nonlinearly distorted multicarrier symbols by iterative decoding," *IEEE Trans. Commun.*, vol. 51, no. 2, pp. 218–228, Feb. 2003.

[31] X. Wang, T. T. Tjhung, and C. S. Ng, "Reduction of peak-to-average power ratio of OFDM systems using a companding technique," *IEEE Trans. Broadcast.*, vol. 45, no. 3, pp. 303–307, Sept. 1999.

[32] X. Huang, J. Lu, J. Zheng, J. Chuang, and J. Gu, "Reduction of peak-to-average power ratio of OFDM signals with companding transform," *IEE Electron. Lett.*, vol. 37, no. 8, pp. 506–507, Apr. 2001.

[33] X. Wang, T. T. Tjhung, and Y. Wu, "On the SER and spectral analyses of A-Law companding multicarrier modulation," *IEEE Trans. Veh. Technol.*, vol. 52, no. 5, pp. 1408–1412, Sept. 2003.

[34] C.-D. Chung and S.-M. Cho, "Constant-envelope orthogonal frequency division multiplexing modulation," in *Proc. APCC/OECC*, vol. 1, Beijing, Oct. 1999, pp. 629–632.

[35] J. Tan and G. L. Stüber, "Constant envelope multi-carrier modulation," in *Proc. IEEE Milcom*, vol. 1, Anaheim, Oct. 2002, pp. 607–611.

[36] S. C. Thompson, J. G. Proakis, and J. R. Zeidler, "Constant envelope binary OFDM phase modulation," in *Proc. IEEE Milcom*, vol. 1, Boston, Oct. 2003, pp. 621–626.

[37] S. C. Thompson, A. U. Ahmed, J. G. Proakis, and J. R. Zeidler, "Constant envelope OFDM phase modulation: spectral containment, signal space properties and performance," in *Proc. IEEE Milcom*, vol. 2, Monterey, Oct. 2004, pp. 1129–1135.

[38] S. C. Thompson, J. G. Proakis, and J. R. Zeidler, "Noncoherent reception of constant envelope OFDM in flat fading channels," in *Proc. IEEE PIMRC*, vol. 1, Berlin, Sept. 2005, pp. 517–521.

[39] Y. Tsai, G. Zhang, and J.-L. Pan, "Orthogonal frequency division multiplexing with phase modulation and constant envelope design," in *Proc. IEEE Milcom*, vol. 4, Oct. 2005, pp. 2658–2664.

[40] R. Pacheco and D. Hatzinakos, "Error rate analysis of phase-modulated OFDM (OFDM-PM) in AWGN channels," in *Proc. IEEE ICASSP*, Toulouse, May 2006, pp. IV337–IV-340.

[41] H. F. Harmuth, "On the transmission of information by orthogonal time functions," *AIEE. Trans.*, vol. 79, pp. 248–255, July 1960.

[42] E. F. Casas and C. Leung, "OFDM for data communication over mobile radio FM channels–part I: analysis and experimental results," *IEEE Trans. Commun.*, vol. 39, no. 5, pp. 783–793, May 1991.

[43] S. Haykin, "Cognitive radio: brain-empowered wireless communications," *IEEE J. Select. Areas Commun.*, vol. 23, no. 2, pp. 201–220, Feb. 2005.

[44] M. Schwartz, W. R. Bennett, and S. Stein, *Communication Systems and Techniques*. McGraw-Hill, 1966.

[45] J. H. Roberts, *Angle Modulation*. London: Peter Peregrinus Ltd., 1977.

[46] J. G. Proakis, *Digital Communications*, 4th ed. New York: McGraw-Hill, 2001.

[47] M. K. Simon and M.-S. Alouini, *Digital Communication over Fading Channels*. New York: John Wiley & Sons, Inc., 2000.

[48] J. G. Proakis and M. Salehi, *Communication Systems Engineering*. New Jersey: Prentice Hall, 1994.

[49] M. Pätzold, *Mobile Fading Channels*. West Sussex, England: John Wiley & Sons, 2002.

[50] J. G. Proakis and D. G. Manolakis, *Digital Signal Processing: Principles, Algorithms, and Applications*, 3rd ed. Upper Saddle River, NJ: Prentice Hall, 1996.

[51] R. E. Ziemer and W. H. Tranter, *Principles of Communications—Systems, Modulation, and Noise*, 4th ed. New York: John Wiley & Sons, 1995.

[52] N. Al-Dhahir, H. Minn, and S. Satish, "Optimum DCT-based multicarrier transceivers for frequency-selective channels," *IEEE Trans. Commun.*, vol. 54, no. 5, pp. 911–921, May 2006.

[53] A. Papoulis, *Probability, Random Variables, and Stochastic Processes*, 3rd ed. Boston, MA: McGraw-Hill, 1991.

[54] H. E. Rowe, *Signals and Noise in Communication Systems*. Princeton, NJ: D. Van Nostrand Company, Inc., 1965.

[55] D. L. Schilling, B. S. Abrams, J. F. Oberst, and M. Berkoff, "Phase locked loop threshold," *Proc. IEEE*, vol. 53, no. 10, p. 1673, Oct. 1965.

[56] J. B. Anderson, T. Aulin, and C.-E. Sundberg, *Digital Phase Modulation*. New York: Plenum Press, 1986.

[57] H. Sari, G. Karam, and I. Jeanclaude, "Transmission techniques for digital terrestrial TV broadcasting," *IEEE Commun. Mag.*, pp. 100–109, Feb. 1995.

[58] I. Kalet, "The multitone channel," *IEEE Trans. Commun.*, vol. 37, no. 2, pp. 119–124, Feb. 1989.

[59] J. Brown and R. Churchill, *Complex Variables and Applications*, 6th ed. McGraw-Hill, 1996.

[60] M. C. Jeruchim, P. Balaban, and K. S. Shanmugan, *Simulation of Communication Systems—Modeling, Methodology, and Techniques*, 2nd ed. New York: Kluwer Academic/Plenum Publishers, 2000.

[61] A. A. M. Saleh, "Frequency-independent and frequency-dependent nonlinear models of TWT amplifiers," *IEEE Trans. Commun.*, vol. 29, no. 11, pp. 1715–1720, Nov. 1981.

[62] S. C. Thompson, J. G. Proakis, and J. R. Zeidler, "The effectiveness of signal clipping for PAPR and total degradation reduction in OFDM systems," in *Proc. IEEE Globecom*, vol. 5, St. Louis, Dec. 2005, pp. 2807–2811.

[63] H. Ochiai, "Performance analysis of peak power and band-limited OFDM system with linear scaling," *IEEE Trans. Wireless Commun.*, vol. 2, no. 5, pp. 1055–1065, Sept. 2003.

[64] C.-P. Liang, J.-H. Jong, W. E. Shark, and J. R. East, "Nonlinear amplifier effects in communications systems," *IEEE Trans. Microwave Theory Tech.*, vol. 47, no. 8, pp. 1461–1466, Aug. 1999.

[65] Xilinx. [Online]. Available: http://www.xilinx.com/

[66] Texas Instruments. [Online]. Available: http://www.ti.com/

Steve C. Thompson (S'00–M'05) was born in Mesa, AZ. He received the B.S. degree from Arizona State University in 1999, the M.S. degree from the University of California, San Diego (UCSD) in 2001, and the Ph.D. degree also from UCSD in 2005, all in electrical engineering.

From 2005 to 2006, Dr. Thompson held a Postdoctoral Scholar position at UCSD, where he collaborated with Nova Engineering (Cincinnati, Ohio) to develop a CE-OFDM prototype. From 2006 to 2007, he was a member of the Advanced Communications Research group at the San Diego Research Center (SDRC). He is currently with Acorn Technologies working on WiMAX development. Dr. Thompson held summer internships at SPAWAR Systems Center (SSC), San Diego in 2001 and 2004, and at the Los Alamos National Laboratory in 1998. His research interests include OFDM, MIMO, modulation, equalization and coding for mobile communication systems.

Ahsen U. Ahmed (S'98) received the B.S. degree from Texas Tech University in 2000 and the M.S. degree from Purdue University in 2002, both in electrical engineering. Currently he is working towards the Ph.D. degree in electrical engineering at the University of California, San Diego (UCSD).

In 2002, he joined SPAWAR Systems Center (SSC), San Diego where he has worked on various satellite and communication systems. He has previously held summer internships at IBM (1998), Space Systems/Loral (2000), and Raytheon (2001). His current research interests include OFDM, modulation, coding, equalization, and their application to various communication systems.

John G. Proakis (S'58–M'62–F'84–LF'99) received the BSEE from the University of Cincinnati in 1959, the MSEE from MIT in 1961 and the Ph.D. from Harvard University in 1967. He is an Adjunct Professor at the University of California at San Diego and a Professor Emeritus at Northeastern University. He was a faculty member at Northeastern University from 1969 through 1998 and held the following academic positions: Associate Professor of Electrical Engineering, 1969-1976; Professor of Electrical Engineering, 1976-1998; Associate Dean of the College of Engineering and Director of the Graduate School of Engineering, 1982-1984; Interim Dean of the College of Engineering, 1992-1993; Chairman of the Department of Electrical and Computer Engineering, 1984-1997. Prior to joining Northeastern University, he worked at GTE Laboratories and the MIT Lincoln Laboratory.

His professional experience and interests are in the general areas of digital communications and digital signal processing. He is the author of the book *Digital Communications* (New York: McGraw-Hill, 2001, fourth edition), and co-author of the books, *Introduction to Digital Signal Processing* (Upper Saddle River: Prentice Hall, 2007, fourth edition); *Digital Signal Processing Laboratory* (Englewood Cliffs: Prentice Hall, 1991); *Advanced Digital Signal Processing* (New York: Macmillan, 1992); *Algorithms for Statistical Signal Processing* (Upper Saddle River: Prentice Hall, 2002); *Discrete-Time Processing of Speech Signals* (New York: Macmillan, 1992, IEEE Press, 2000); *Communication Systems Engineering* (Upper Saddle River: Prentice Hall, 2002, second edition); *Digital Signal Processing Using MATLAB V.4* (Boston: Brooks/Cole-Thomson Learning, 2007, second edition); *Contemporary Communication Systems Using MATLAB* (Boston: Brooks/Cole-Thomson Learning, 2004, second edition); and *Fundamentals of Communication Systems* (Upper Saddle River: Prentice Hall, 2005).

James R. Zeidler (M'76–SM'84–F'94) is a Research Scientist/Senior Lecturer in the Department of Electrical Engineering at the University of California, San Diego. He is a faculty member of the UCSD Center for Wireless Communications and the University of California Institute for Telecommunications and Information Technology. He has more than 200 technical publications and thirteen patents for communication, signal processing, data compression techniques, and electronic devices.

Dr. Zeidler was elected Fellow of the IEEE in 1994 for his technical contributions to adaptive signal processing and its applications. He received a best paper award at the 2006 IEEE Personal, Indoor, and Mobile Radio Conference; the Frederick Ellersick best paper award from the IEEE Communications Society at the IEEE Military Communications Conference in 1995; the Navy Meritorious Civilian Service Award in 1991; and the Lauritsen-Bennett Award for Achievement in Science from the Space and Naval Warfare Systems Center in 2000. He was an Associate Editor of the IEEE TRANSACTIONS ON SIGNAL PROCESSING.

Michael J. Geile (S'83–M'91) was born in St. Johns, Missouri in 1960. He received a M.S. in electrical engineering from The Ohio State University in 1996. He was a co-inventor of the HD Radio OFDM waveform and has developed over six OFDM implementations in the past 10 years including definition of the constant envelope OFDM developed under an ONR sponsorship and the JTRS WNW OFDM physical layer waveform. Michael's current research interests include multipath and interference mitigation applied to wireless networks. Currently, Michael is the Chief Technical Officer of Nova Engineering in Cincinnati, Ohio.